Applied Thermal Engineering 212 (2022) 118530

Contents lists available at ScienceDirect

Applied Thermal Engineering

journal homepage: www.elsevier.com/locate/apthermeng

Research Paper

Thermal and electrical characterization of an electric vehicle battery cell, an experimental investigation

Sahin Gungor [a,b,c], Erdal Cetkin [b], Sylvie Lorente [a,*]

[a] Villanova University, Department of Mechanical Engineering, Villanova, PA 19085, USA
[b] Izmir Institute of Technology, Department of Mechanical Engineering, 35430, Turkey
[c] Izmir Katip Celebi University, Department of Mechanical Engineering, 35620, Turkey

ARTICLE INFO

Keywords:
Electric vehicle
Li-ion batteries
Thermal characteristics
Capacity fade
Experimental results

ABSTRACT

This paper documents the experimental characterization of a Li-ion battery cell during charging/discharging cyclic operations. The study of the battery cell is conducted in the absence of cooling aid system, and provides thermal and electrical insights. After describing the experimental set-up, the changes in temperature are presented and highlight the nonuniform distribution of the temperature on the battery cell surface. The findings indicate that the maximum temperature difference on the investigated battery cell surface may reach up to 11 C at 3C and 17 °C at 5C, at the end of the discharge in the natural convection case. These changes in space come with temporal variations that are also documented. Voltage curves are provided during charging and discharging operations. The impact of the discharge rate, ambient temperature are then investigated together with the capacity fade after 500 cycles, and results showed that ventilation and low ambient temperatures allow to alleviate the battery capacity fade by 3%.

1. Introduction

Electric and hybrid vehicle technologies contribute to reducing carbon emissions and are perceived as an eco-friendly solution for transportation [1]. They do not come without some challenges though: ensuring fast charging, heat generation-based safety risks, and milage range issues are the most crucial ones. The batteries used in electric vehicles (EV) are rechargeable power sources in which stored chemical energy is converted into electricity. Today, Li-ion based batteries are considered to be the most advanced technology by the EV companies [2,3]. Li-ion batteries consist of positive–negative electrodes, electrolyte layer, porous separator, positive–negative collectors, and tab sections. The electrochemical reaction speed, the layer purity, the internal resistance, the aspect ratio of the layers structure, the tab location, and the operating temperature are the most influential factors on the Li-ion battery performance and operating stability [4–6]. Because the time for charging the battery is key, the C-rate is another important parameter. The C-rate represents measurement of the charge and discharge current with respect to its nominal capacity; the higher the C-rate, the faster the time for charge/discharge. Nevertheless, high C-rates lead to increased heat generation within the Li-ion battery cell.

Heat generation within a battery cell may cause solid-electrolyte interface degradation and even thermal runaway [7–9]. The latter can be considered as a chain electrochemical reaction in which a temperature increment triggers the reaction speed, and vice versa. Even in the absence of thermal runaway, the heat generation during the charge and discharge also accelerates the battery capacity losses [10,11]. Capacity fade mainly effects the battery performance and impacts the EV milage range. The capacity fade within the EV battery pack depends on the operating temperature, the total number of charge/discharge cycles, and the C-rate [11–14]. Hunt et al. [15] experimentally investigated the capacity fade of 5 Ah pouch type Li-ion battery cells under various thermal management techniques of Peltier element, forced air, and tab cooling. The cells were tested up to 1000 cycles with 2C fast charging. The discharge rate was varied between C/20, 1C, and 6C. The results indicated that increasing the discharge rate accelerates the capacity fade, as expected. Wang et al. [16] documented the capacity fade of 1.5 Ah cylindrical Li-ion battery cells discharged between 0.5C and 6.5C, and they proposed correlations in the capacity fade based on the number of cycles.

on the capacity fade based on time and number of cycles. The temperature range varied from 10 °C to 46 °C to observe the effects of the operating temperature on the capacity fade. The proposed correlations were used by Gennaro et al. [17] for the Nickel-Cobalt-Manganese oxide (NCM) battery cells, and they also reviewed all the other capacity fade

* Corresponding author.
E-mail address: sylvie.lorente@villanova.edu (S. Lorente).

https://doi.org/10.1016/j.applthermaleng.2022.118530
Received 7 January 2022; Received in revised form 5 April 2022; Accepted 12 April 2022
Available online 15 April 2022
1359-4311/

Nomenclature

C	C-rate
h	convective heat transfer coefficient [$Wm^{-2} K^{-1}$]
Nu	Nusselt number
Pr	Prandtl number
Q	capacity [Ah]
Ra	Rayleigh number
Re	Reynolds number
R^2	goodness of fit [dimensionless]
t	time [s]
T	temperature [K]
$\overline{T}$	average temperature [K]

Subscripts

amb	ambient
cycle	based on charge/discharge cycle
final	value at the end of operation
H	value based on height
loss	capacity fade
throughput	total amount of ampere-hours exchanged by the battery cell during the cycles
1	first thermocouple region
2	second thermocouple region
3	third thermocouple region

Abbreviations

CC-CV	constant current-constant voltage
DoD	depth of discharge
EC	ethylene carbonate
EMC	ethyl methyl carbonate
EV	electric vehicle
FC	forced convection
Li	lithium
$LiPF_6$	lithium hexafluorophosphate
NC	natural convection
NCM	nickel–cobalt-manganese
SoC	state of charge

correlations in the literature for the various cell chemistries. Note that strict thermal control minimizes the operational capacity losses of the EV battery packs. At this point, literature has comprehensive research papers related to the investigation of battery thermal-electrical characteristics and thermal management solutions [18–20].

While the literature offers many experimental results on the battery cells capacity fade or, to a lesser extent, on cooling solutions, there is a lack of measurements of the temperature distribution in time and space on battery cells during charging and discharging coupled with electrical measurements, in the absence of any cooling aid. After a first publication coupling experimental and numerical work [21], this paper documents the experimental characterization of a pouch type Li-ion battery cell during charging/discharging cyclic operations. After describing the experimental set-up, the changes in temperature and voltage are given in charging and discharging conditions. The impact of the discharge rate, ambient temperature are then investigated together with the capacity fade.

2. Experiments

We tested a Kokam SLPB75106100 Li-ion battery. Its main characteristics are summarized in Table 1.

The experimental conditions consisted in placing the battery cell in a chamber at controlled constant temperature, T_{amb}. Two cases were considered: T_{amb}= 25 °C, and T_{amb} = 40 °C. The latter corresponds to the maximum temperature that the battery can undergo before degradation [22,23]. A ventilation system in the chamber allowed to generate an airflow around the cell. We termed this configuration as Forced Convection (FC). We were able to determine the corresponding convection heat transfer coefficient by measuring the air velocity with a digital anemometer located just above the battery cell. The air velocity was time-averaged over a 1-minute period to prevent instant measurement errors. During other tests, the ventilation system was turned off, the air flow was due only to buoyancy in the vicinity of the battery cell which was generating heat during the different phases of charge and discharge.

Table 1
Main properties of the pouch cell.

Dimensions (mm)	Electrode materials	Electrolyte mixture	Nominal voltage (V)	Capacity (Ah)
107 × 102 × 7.2	NCM-graphite	EC/EMC/$LiPF_6$	3.7	7.5

Such case is named the Natural Convection (NC) case. Two identical battery cells were charged at a 2C rate and discharged at a 3C rate and 5C rate respectively.

The two experimental set-ups are shown in Fig. 1a (set-up A) and 1b (set-up B). Set-up A mainly contains a programmable DC power supply for charging (Chroma 62024P model, 2400 W/100 V/50A), two different electronic loads for discharging (Prodigit 3332F model, 120

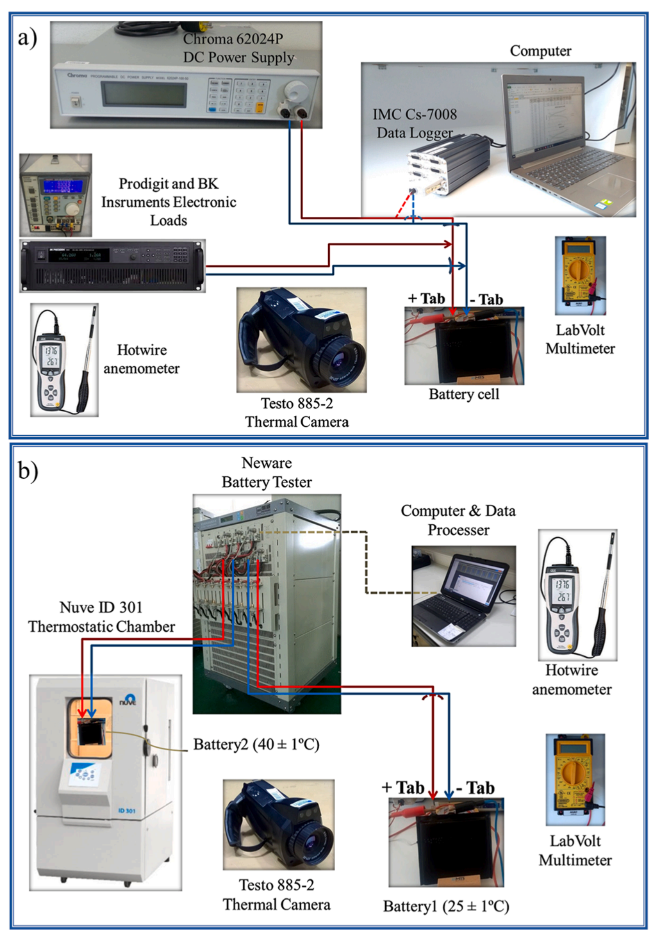

Fig. 1. Li-ion battery cell test configurations, (a) set-up A and (b) set-up B.

W/80 V/24A and BK Instruments Precision model, 1500 kW/120 V/240A), a data-logger for collecting the voltage data (IMC Cs-7008 model, 8-channels), a thermal imager (Testo 885–2 model, temperature sensitivity ≤ 0.03 °C with an IR resolution of 240 × 320 pixels) for capturing the Li-ion cell surface temperature map, and a digital multimeter (Lab-Volt 6394A model) to double-check the voltage and current values.

The set-up B is identical to the set-up A, and includes also a Li-ion battery cycler (Neware BTS4000 high power series, 50 V/100A) for the capacity fade experiment. We used set-up A when discharging the battery cell at 3C and 5C rates under natural convection conditions at the ambient temperature of 25 °C. The temperature maps during the discharge process were captured every 0.3 s with a Testo 885–2 thermal imager. Note that the battery cells were coated with matte black paint to increase the emissivity of the surface and to disable reflection of the thermal radiation. The voltage data were collected via a multichannel data-logger (Fig. 1a) with a precision of 1 s. The limits for the cut-off (2.8 V) and maximum (4.2 V) voltage were determined in accordance with the Kokam battery cell user manual [24].

3. Verification

To control the results, we also placed three thermocouples towards the positive tab location (Thermocouple 1), in the middle of the cell surface (Thermocouple 2), and connected to the positive and negative tabs (Thermocouple 3). The thermocouples 1 and 2 provided the temperature changes during the charging and discharging process, while the third thermocouple collected the voltage changes (Fig. 2). A thermally insulated tape was used to maintain the thermocouples.

We present in Fig. 3 the temperature changes during the discharge at the level of the positive tab (Fig. 3a) and in the middle of the surface (Fig. 3b) for 3C and 5C rates when the ambient temperature is 25 °C in natural convection. The curves in red correspond to the results provided by the thermocouples while the blue ones give the temperature values from the thermal camera. In the latter, we allocated a square region of 1 cm^2 centered on the thermocouple, and considered the average temperature. The results for the voltage change are shown in Fig. 4. Note that the temperature and voltage curves obtained with the thermocouples are very similar to the ones with the thermal camera and voltmeter.

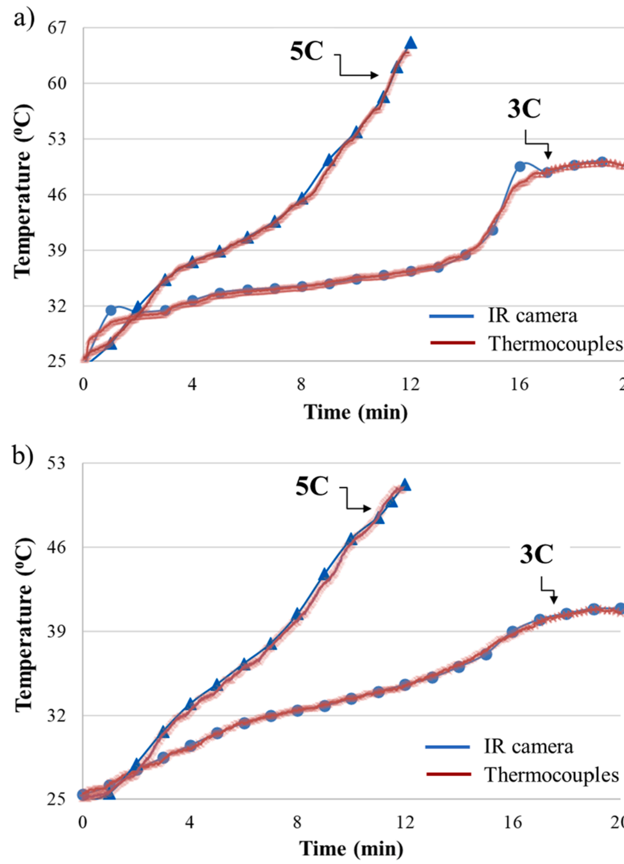

Fig. 3. Thermal camera and thermocouple measurements for 3C and 5C discharge rates (a) in the tab section and (b) in the middle of the battery cell. T_{amb} = 25 °C, NC configuration.

4. Battery voltage and temperature

4.1. Charging and discharging

The two identical Li-ion battery cells were exposed to the same fast charging rate (2C) and a discharging rate of 3C for one cell and 5C for the other one at T_{amb} = 25 °C, in the natural convection configuration.

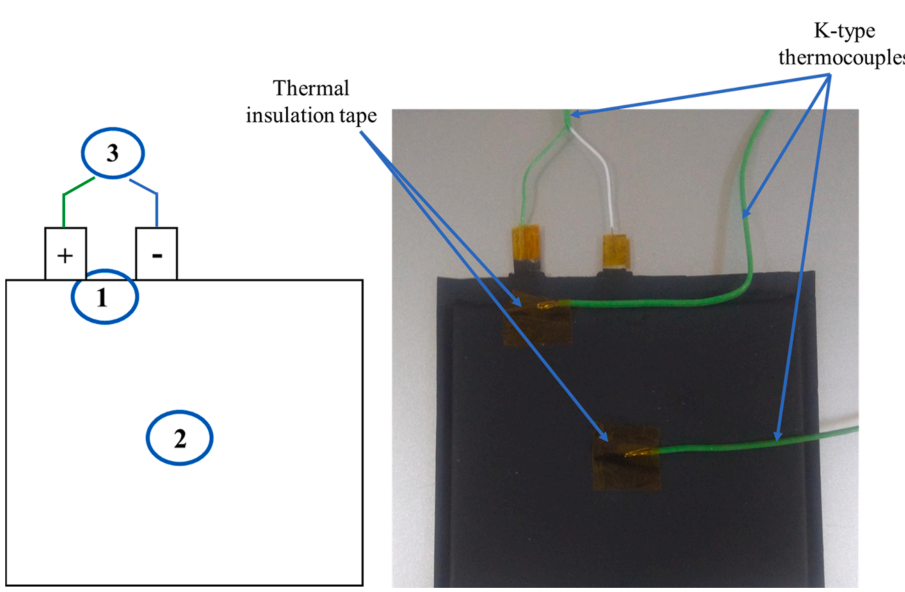

Fig. 2. Thermocouple locations on the Li-ion battery cell.

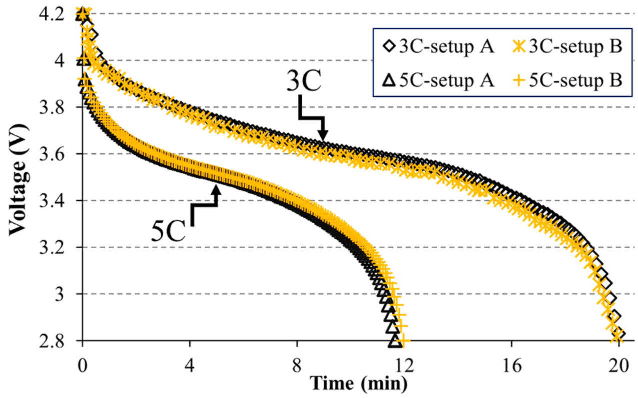

Fig. 4. Voltage curves under 3C and 5C discharge rates. T_{amb} = 25 °C, NC configuration.

The charge and discharge rates were determined according to the limits recommended by the manufacturer [24] for safe and continuous operations. Fig. 5 provides the voltage curves of the battery cell during the charging and discharging processes. The discharging rate is 3C in Fig. 5a and 5C in Fig. 5b. We added to the graph the temperature maps captured at the end of the charge and discharge operations for the sake of illustration.

The fast-charging operation took about 45 min with a constant current-constant voltage (CC– CV) protocol, while the 3C and 5C discharge processes lasted about 20 min and 12 min, respectively. Regardless the time for discharge, the shape of the discharge curves is similar. Yet, the temperature levels are quite different, as detailed in the next sections of the paper.

4.2. History of the temperature changes

We captured thermal videos to determine the temperature variations from $t = 0$ to $t = t_{final}$ when the two identical cells were discharged at 3C and 5C rates, in the natural convection configuration at $T_{amb} = 25$ °C. The thermal camera allows to record images approximately every 0.15 s. For more insights, the thermal movie of the 3C discharge process is attached as the supplementary material (appendix A).

Fig. 6 presents a sample of the temperature distributions on the battery cell surface with respect to the depth of discharge (DoD) levels for the 3C discharge process (left-hand side) and for the 5C case (right-hand side). The images correspond to the measurements at 25%, 50%, 75% and 100% of DoD. We chose to use a common set of colors for the temperature range to illustrate the effect of the discharge rate on the temperature distribution. In both cases, the battery cell starts heating immediately as soon as the discharge starts, especially towards the

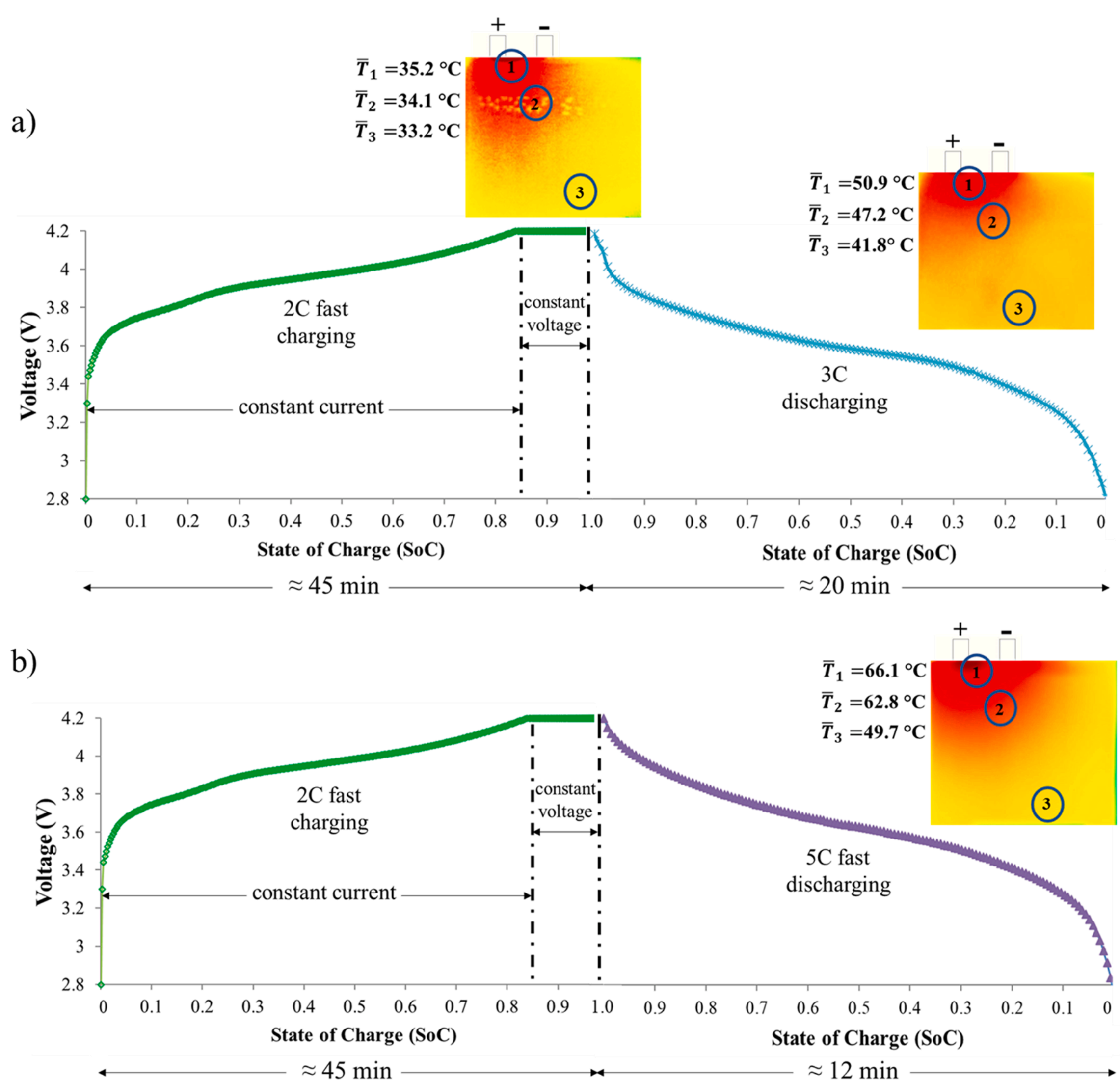

Fig. 5. Voltage curves of 2C rate in fast charging mode, and (a) 3C, (b) 5C rates discharging modes, T_{amb}= 25 °C, NC configuration.

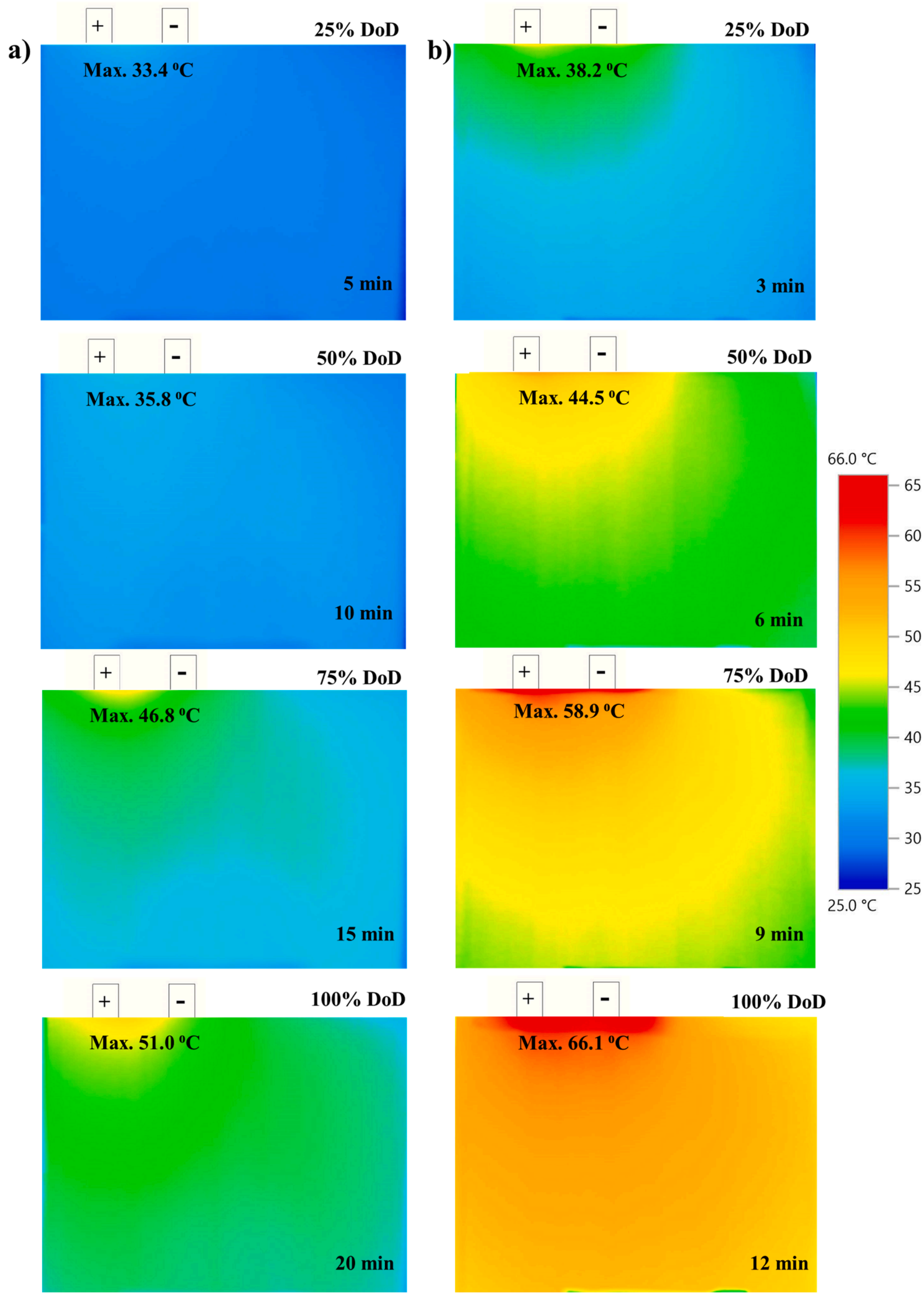

Fig. 6. Temperature maps of (a) 3C and (b) 5C discharge operations at 25%, 50%, 75%, and 100% depth of discharge (DoD), NC configuration, T_{amb} = 25 °C.

positive tab. The thermal wave propagates from the tabs to the entire cell surface in a similar fashion, regardless the discharge value. The heat diffusion is overall radial. The temperature maps in Fig. 6 highlight that the difference between the two discharge cases lies in the amplitude of the temperature change, not in the way heat propagates.

4.3. Impact of the rate of discharge

Detecting changes in the cell temperature levels at various discharge rates is crucial to design effective battery thermal control systems, and contributes to the lifetime, performance, and co-aging of the electric vehicle batteries. The current is the dominant factor affecting the thermal and electrical behavior of the Li-ion cells. Higher charge and discharge rates correspond to higher current densities, and this triggers the electrochemical reaction kinetics and the heat generation within the cell.

As shown in Fig. 6, the temperature in the vicinity of the battery tabs increases of about 7.6 °C (3C discharge) and 11 °C (5C discharge) at 25%

DoD. The maximum temperature was obtained at the end of the discharge operation (100% DoD). It was located around the positive tab and measured at 50.9 °C (3C discharge) and 66.1 °C (5C discharge). The temperature difference between the top and bottom of the battery cell also increased with respect to the DoD level. The maximum temperature difference was about 11 °C (3C discharge) and 17 °C (5C discharge) when the battery cell was fully discharged. This latter value is far beyond the admissible temperature difference of 5 °C [25].

4.4. Impact of the ambient temperature

One battery cell was tested in set-up B with the ambient temperature maintained at 40 ± 1 °C, and without any cooling aid. This natural convection case was compared to the results obtained with an ambient temperature at 25 °C. Fig. 7 presents the temperature distribution at the surface of the battery cell when the thermostatic chamber temperature is kept at 25 °C (Fig. 7a) and 40 °C (Fig. 7b). The thermal maps correspond to the end of the discharge at a 5C rate. As shown in the figure, the temperature distribution is non-uniform with a hot spot located in the vicinity of the tabs in both cases. When the battery cell is placed in a warmer environment, its maximum surface temperature is increased of 3.4 °C compared to the case with an ambient temperature at 25 °C, going from 66.1 °C to 69.5 °C. The temperature increase was higher in the middle and in the lower part of the cell. This increase is 7.4 °C and 6.6 °C respectively, going from an ambient temperature of 25 °C to 40 °C.

Note that the ambient temperature impacts the kinetics of the electrochemical reaction, and therefore the change in temperature level at the surface of the battery cell can not be predicted directly from the change in ambient temperature. Here, the maximum temperature difference at the cell surface (between top and bottom) decreases when the surrounding ambient temperature changes from 25 °C to 40 °C, indicating a more homogenous temperature distribution on the cell surface when $T_{amb} = 40$ °C. This phenomenon results from the lower but more uniform heat generation during the discharging operation in the 40 °C case relative to the 25 °C [26,27].

Fig. 7 also presents the voltage measurements during the discharge process for the two ambient temperatures. The voltage curve obtained with $T_{amb} = 40$ °C is always located above the one corresponding to the 25 °C ambient temperature conditions. This is particularly true at the beginning of the discharging process. The difference between the two curves tends to decrease when the DoD reaches 40%. Note that the battery cell capacity was measured at 7.29 Ah when $T_{amb} = 25$ °C, and 7.47 Ah when $T_{amb} = 40$ °C at the beginning of the discharging operations (0% DoD).

4.5. Impact of the environmental conditions

Until this point, we have presented the experimental results under natural convection conditions. The natural convection heat transfer coefficients for the ambient temperature of 25 °C can be estimated at 12.8 W/m^{2}K from $Nu = 0.59Ra_H^{1/4}$, when the Rayleigh number based on the wall height remains below 10^9 [28,29]. We also investigated the thermal and electrical behaviors of an identical Li-ion cell when the battery surfaces are exposed to forced convection under a discharge rate of 5C. The battery surface was swept by air blown by a fan at 25 °C. The time-averaged air velocity was measured as 2.1 m/s. The measurements were performed with a digital anemometer probe (hotwire) located just above the battery cell. The convective heat transfer coefficient was calculated from $Nu = 0.664Re_H^{1/2}Pr^{1/2}$, a correlation in forced convection with $Re_H = 1.3 \times 10^4$ [28,29] leading to a value of 35.6 W/m^{2}K.

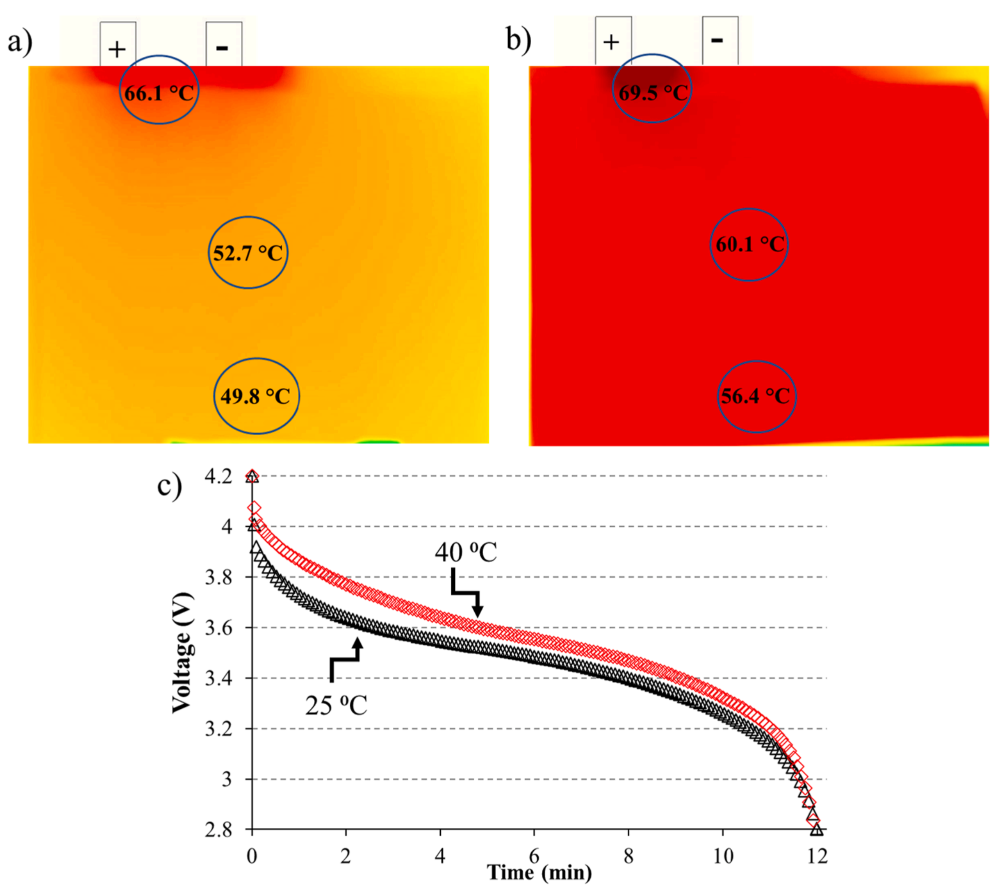

Fig. 7. Temperature distribution on the battery surface at ambient temperatures of (a) 25 °C and (b) 40 °C, (c) voltage curves in a 5C discharge case, NC configuration.

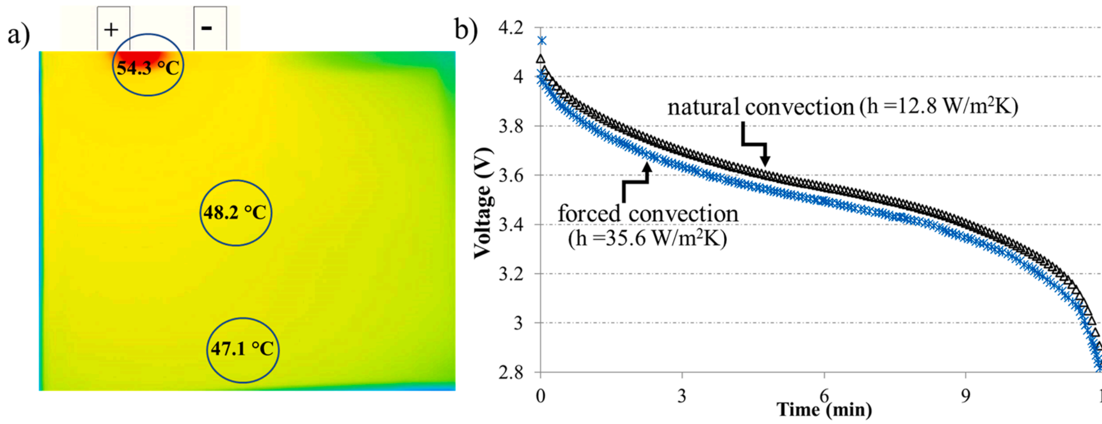

Fig. 8. FC results, (a) temperature map and (b) voltage curves, 5C discharge, $T_{amb} = 25$ °C.

Fig. 8 shows the temperature map and voltage curve of the investigated battery cell under the forced convection condition.

The thermal map was measured at the end of the discharge process. The trends in the temperature distribution given in Fig. 8a is very similar to the natural convection results (Fig. 7a). Yet, the temperature levels decreased of about 11.8 °C thanks to the air mixing by forced convection which leads to a heat transfer coefficient three times higher than in natural convection. Hotspot regions were observed in the vicinity of the battery tabs, while the temperature dropped towards the bottom section of the cell. The voltage curves corresponding to the natural and forced convection conditions are presented in Fig. 8b. The two behaviors are almost identical.

5. Capacity fade

The capacity fade of the two identical Li-ion battery cells was investigated for 500 cycles. The tests were conducted via the experimental set-up B (Fig. 1) which includes a battery cycler. Each cycle consisted in charging at 2C and discharging at 5C. We chose to consider the case of $T_{amb} = 25$ °C in forced convection and $T_{amb} = 40$ °C in natural convection, considering that this would lead to the most extreme results in the range of temperature chosen.

The initial capacities of the cells, which were never used previously, were noted at the beginning of the experiment. They were measured at 7.28 Ah (cell at $T_{amb} = 25$ °C) and 7.47 Ah (cell at $T_{amb} = 40$ °C). A higher nominal capacity was observed in the 40 °C scenario since the Li-ion battery capacity is a function of the battery cell temperature. Then, we measured and logged the remained capacity of the cells after each cycle. Table 2 presents the capacity fade results of each investigated condition. The initial capacity of the battery cells at 25 °C and 40 °C decreased of about 8.5% and 11.8% at the end of 500 cycles, respectively. The results indicate that the total capacity fade after 500 cycles can be reduced by 3.3% with lower operating temperature. Wang et al. [16] investigated Li-ion cells with a chemistry (NCM, nickel–cobalt-manganese) similar to our batteries and measured the capacity fade under various C-rates and ambient temperatures. The results were documented by Gennaro et al. [17].

Table 2
Capacity fade results.

Cycles	Cell capacity (Ah) $T_{amb} = 25$ °C	$T_{amb} = 40$ °C
0	7.29	7.47
100	6.9	7.23
200	6.82	7.13
300	6.78	6.95
400	6.72	6.77
500	6.67	6.59

The capacity fade data of the 5C discharge operation presented in Ref. 16 are plotted in Fig. 9 for the operating temperatures of 10 °C, 34 °C, and 46 °C. We added our experimental values in the same figure. The lower ambient temperatures are separated from the higher ones: Fig. 9a shows the results when $T_{amb} \leq 34$ °C, while measurements for $T_{amb} \geq 34$ °C are reported in Fig. 9b. The results indicate that the capacity fade curves follow the same trend as the literature results. After 500 cycles, the cell loses more capacity when the environment temperature increases.

We used the following correlation based on the number of cycles [16,17]:

$$Q_{loss-cycle} = \left(aT^2 + bT + c\right).e^{[(dT+e)C_{rate}]}.Ah_{throughput} \quad (1)$$

where $Q_{loss-cycle}$ is the percentage of capacity loss, T is the temperature in Kelvin, $Ah_{throughput}$ is the total amount of ampere-hours exchanged by the battery cell during the cycles. Note that the C-rate determines the trend of this exponential relation.

Relying on the correlation presented in Eq. (1), we determined the set of coefficients (a to e) via a code developed in Wolfram Mathematica. The code was written for statistical evaluation and curve fitting of the data set. Note that the proposed correlation is based on the experimental capacity fade results (Table 2), the two ambient temperatures, the C-rate, and the total $Ah_{throughput}$ during the cycles. In addition, we tested the statistical success (R^2 and adjusted-$R^2 \geq 0.99$) and fitting stability of the correlation by the aid of the developed code. The correlation coefficients are documented in Table 3.

Identical batteries manufactured by the same company may have dissimilar internal resistance and electrochemical reaction characteristics as the batteries rely on multi-physics at macro, micro, and nanoscale levels. Among battery cells of similar composition local capacity fade differences can result from many factors such as the layer purity of the electrodes and electrolyte, the battery cell nominal capacity, the tabs material and their location, the local hotspots based on the electrical connections etc. The capacity fade results obtained experimentally are in good agreement with the literature correlation [16,17]. A slight change in the coefficients c and d in Eq. (1) allow to follow with a better accuracy the experimental trends both at 25 °C and 40 °C.

6. Conclusion

The thermal and electrical characterization of the Li-ion battery cell, under various boundary conditions (25 °C and 40 °C ambient temperature, natural and forced convection) allows to draw the following concluding remarks:

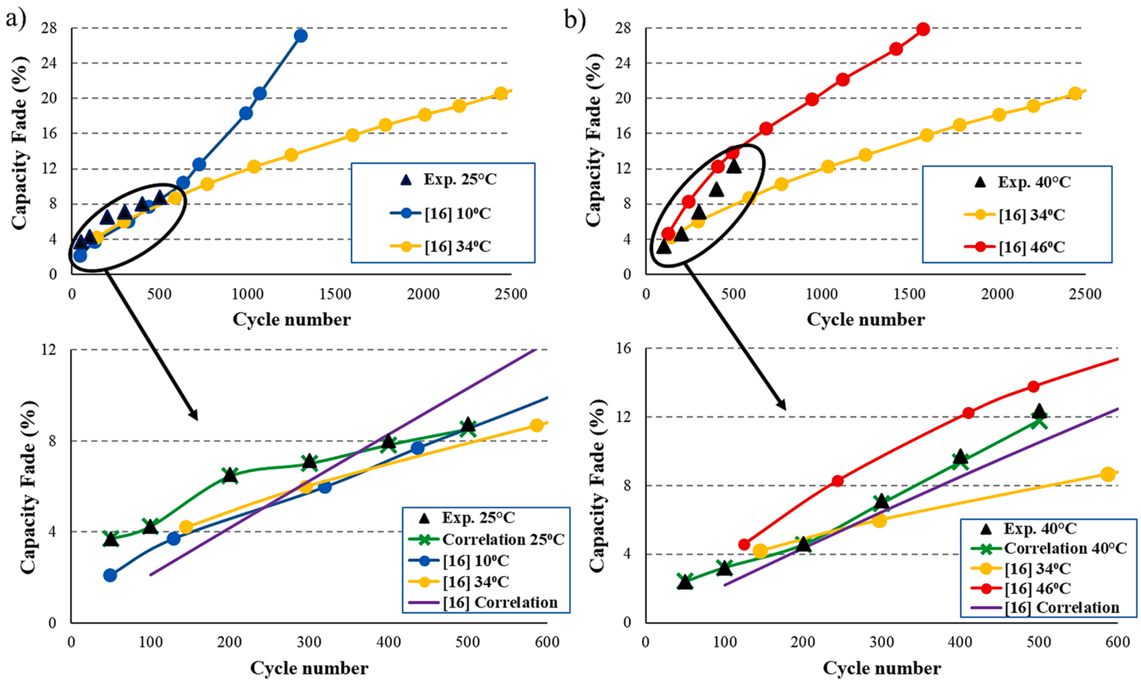

Fig. 9. Comparison of the experimental capacity fade results and literature data for environmental conditions of 25 °C in FC (left) and 40 °C in NC (right).

Table 3
Coefficients in Eq. (1).

Coefficients	Unit	Wang et al. [16]	Present work
a	$Ah^{-1}K^{-2}$	8.61×10^{-6}	8.61×10^{-6}
b	$Ah^{-1}K^{-1}$	-5.13×10^{-3}	-5.13×10^{-3}
c	Ah^{-1}	7.63×10^{-1}	7.732×10^{-1}
d	$K^{-1}C_{rate}^{-1}$	-6.7×10^{-3}	-2.973×10^{-3}
e	C_{rate}^{-1}	2.35	2.35

1- The Li-ion battery cells have a nonhomogeneous temperature distribution caused by the nonuniform heat generation within the cells. In this study, the maximum temperature difference on the battery cell surface reached up to 11 °C at 3C and 17 °C at 5C, at the end of the discharge in the natural convection case.
2- Hotspots were observed in the vicinity of the battery tabs due to the higher current density. The evolution of the temperature maps at different discharge rates was captured via thermal movies (appendix A). Heat propagates from the tabs toward the opposite side of the cell. The C-rate impacts the temperature level but not the heat propagation pattern. When the ambient temperature moves from 25 °C to 40 °C, a significant effect on the battery cell surface temperature is noticed. But it does not translate into effect on the voltage curve during the discharge.
3- Adding ventilation around the cell allows to lower temperature at the cell surface without significant impact on the voltage change in discharge. Ventilation and low ambient temperatures allow to alleviate the battery capacity fade by 3% at the end of 500 cycles of charge/discharge.

Declaration of Competing Interest

The authors declare the following financial interests/personal relationships which may be considered as potential competing interests: Sahin Gungor reports financial support was provided by Scientific and Technological Research Council of Turkey.

Acknowledgement

The authors would like to acknowledge the Scientific and Technological Research Council of Turkey (TUBITAK) support program with the grant numbers of 218M498 and 1059B142000143.

Appendix A

Thermal movie of the 3C discharge operation.

Appendix B. Supplementary material

Supplementary data to this article can be found online at https://doi.org/10.1016/j.applthermaleng.2022.118530.

References

[1] Y. Li, Z. Zhou, W.T. Wu, Three-dimensional thermal modeling of Li-ion battery cell and 50 V Li-ion battery pack cooled by mini-channel cold plate, App. Therm. Eng. 147 (2019) 829–840, https://doi.org/10.1016/j.applthermaleng.2018.11.009.
[2] M. Walter, M.V. Kovalenko, K.V. Kravchyk, Challenges and benefits of post-lithium-ion batteries, New J. Chem. 44 (2020) 1677–1683, https://doi.org/10.1039/c9nj05682c.
[3] Post Lithium-ion Batteries, https://www.nature.com/collections/bsctnmnrtc. (Accessed: 03 March 2022).
[4] D. Lee, J. Lee, J. Kim, S. Cho, C.W. Kim, Thermal behaviors analysis of 55 Ah large-format lithium-ion pouch cells with different cell aspect ratios, tab locations, and C-rates, App. Therm. Eng. 175 (2020) 115422, https://doi.org/10.1016/j.applthermaleng.2020.115422.
[5] Z. Lu, X.L. Yu, L.C. Wei, F. Cao, L.Y. Zhang, X.Z. Meng, L.W. Jin, A comprehensive experimental study on temperature-dependent performance of lithium-ion battery, App. Therm. Eng. 158 (2019) 113800, https://doi.org/10.1016/j.applthermaleng.2019.113800.
[6] S. Ma, M. Jiang, P. Tao, C. Song, J. Wu, J. Wang, T. Deng, W. Shang, Temperature effect and thermal impact in lithium-ion batteries: A review, Prog. Nat. Sci-Mat. 28 (2018) 653–666, https://doi.org/10.1016/j.pnsc.2018.11.002.
[7] A. García, J.M. Serrano, R.L. Sari, S.M. Boggio, Influence of environmental conditions in the battery thermal runaway process of different chemistries: Thermodynamic and optical assessment, Int. J. Heat Mass Transf. 184 (2022) 122381, https://doi.org/10.1016/j.ijheatmasstransfer.2021.122381.
[8] Z. Lei, Z. Maotao, X.u. Xiaoming, G. Junkui, Thermal runaway characteristics on NCM lithium-ion batteries triggered by local heating under different heat dissipation conditions, Applied Thermal Engineering 159 (2019) 113847, https://doi.org/10.1016/j.applthermaleng.2019.113847.

[9] A. García, J.M. Serrano, R.L. Sari, S.M. Boggio, Thermal runaway evaluation and thermal performance enhancement of a lithium-ion battery coupling cooling system and battery sub-models, Appl. Therm. Eng. 202 (2022) 117884, https://doi.org/10.1016/j.applthermaleng.2021.117884.
[10] G. Jiang, L. Zhuang, Q. Hu, Z. Liu, J. Huang, An investigation of heat transfer and capacity fade in a prismatic Li-ion battery based on an electrochemical-thermal coupling model, Appl. Therm. Eng. 171 (2020) 115080, https://doi.org/10.1016/j.applthermaleng.2020.115080.
[11] M. Xu, R. Wang, P. Zhao, X. Wang, Fast charging optimization for lithium-ion batteries based on dynamic programming algorithm and electrochemical-thermal-capacity fade coupled model, J. Power Sources 438 (2019) 227015, https://doi.org/10.1016/j.jpowsour.2019.227015.
[12] A. Carnovale, X. Li, A modeling and experimental study of capacity fade for lithium-ion batteries, Energy and AI 2 (2020) 100032, https://doi.org/10.1016/j.egyai.2020.100032.
[13] P. Marques, R. Garcia, L. Kulay, F. Freire, Comparative life cycle assessment of lithium-ion batteries for electric vehicle addressing the capacity fade, J. Clean. Product. 229 (2019) 787–794, https://doi.org/10.1016/j.jclepro.2019.05.026.
[14] S. Saxena, C.L. Floch, J. Macdonald, S. Moura, Quantifying EV battery end-of-life through analysis of travel needs with vehicle powertrain models, J. Power Sources 282 (2015) 265–276, https://doi.org/10.1016/j.jpowsour.2015.01.072.
[15] I.A. Hunt, Y. Zhao, Y. Patel, J. Offer, Surface cooling causes accelerated degradation compared to tab cooling for lithium-ion pouch cells, J. Electrochem. Soc. 163 (9) (2016) A1846–A1852.
[16] J. Wang, J. Purewal, P. Liu, J. Hicks-Garner, S. Soukazian, E. Sherman, A. Sorenson, L. Vu, H. Tataria, M.W. Verbrugge, Degradation of lithium-ion batteries employing graphite negatives and nickel-cobalt-manganese oxide+spinel manganese oxide positives: Part 1, aging mechanisms and life estimation, J. Power Sources 269 (2014) 937–949, https://doi.org/10.1016/j.jpowsour.2014.07.030.
[17] M. De Gennaro, E. Paffumi, G. Martini, A. Giallonardo, S. Perdroso, A.L. Lapointe, A case study to predict the capacity fade of the battery of electrified vehicles in real-world use conditions, Case. Stud. 8 (2020) 517–534, https://doi.org/10.1016/j.cstp.2019.11.005.
[18] M.K. Tran, S. Panchal, V. Chauhan, N. Brahmbhatt, A. Mevawalla, R. Fraser, M. Fowler, Python-based scikit-learn machine learning models for thermal and electrical performance prediction of high-capacity lithium-ion battery, Int. J. Energy Res. 46 (2022) 686–794, https://doi.org/10.1002/er.7202.
[19] C. Akkaldevi, S.D. Chitta, J. Jaidi, S. Panchal, M. Fowler, R. Fraser, Coupled electrochemical-thermal simulations and validation of minichannel cold-plate water-cooled prismatic 20 Ah LiFePO4 Battery, Electrochem 2 (2021) 643–663, https://doi.org/10.3390/electrochem2040040.
[20] V.G. Choudhari, A.S. Dhoble, S. Panchal, M. Fowler, R. Fraser, Numerical investigation on thermal behavior of 5× 5 cell configured battery pack using phase change material and fin structure layout, J. Energy Stor. 43 (2021) 103234, https://doi.org/10.1016/j.est.2021.103234.
[21] S. Gungor, E. Cetkin, S. Lorente, Canopy-to-canopy liquid cooling for the thermal management of lithium-ion batteries, a constructal approach, Int. J. Heat Mass Trans. 182 (2022) 121918, https://doi.org/10.1016/j.ijheatmasstransfer.2021.121918.
[22] N. Omar, Y. Firouz, H. Gualous, J. Salminen, T. Kallio, J.M. Timmermans, T. Coosemans, P. Van den Bossche, J. Van Mierlo, Aging and degradation of lithium-ion batteries, Rechargeable Lithium Batteries (2015) 263–279, https://doi.org/10.1016/B978-1-78242-090-3.00009-2.
[23] M.K. Rahman, Y. Saito, Investigation of positive electrodes after cycle testing of high-power Li-ion battery cells: III: An approach to the power fade mechanism using FT-IR-ATR, J. Power Sources 174 (2007) 889–894, https://doi.org/10.1016/j.jpowsour.2007.06.222.
[24] Kokam Li-ion cell brochure, https://kokam.com/wp-content/uploads/2016/03/SLPB-Cell-Brochure.pdf. (Accessed: 02 Mar 2022).
[25] A.A. Pesaran, Battery thermal models for hybrid vehicle simulations, J. Power Sources 110 (2) (2002) 377–382, https://doi.org/10.1016/S0378-7753(02)00200-8.
[26] L. Shenga, L. Sua, H. Zhangb, Y. Fanga, H. Xua, W. Yec, An improved calorimetric method for characterizations of the specific heat and the heat generation rate in a prismatic lithium-ion battery cell, Energy Conv. Man. 180 (2019) 724–732, https://doi.org/10.1016/j.enconman.2018.11.030.
[27] Y. Xie, S. Shi, J. Tang, H. Wuc, J. Yu, Experimental and analytical study on heat generation characteristics of a lithium-ion power battery, Int. J. Heat Mass Trans. 122 (2018) 884–894, https://doi.org/10.1016/j.ijheatmasstransfer.2018.02.038.
[28] F.P. Incropera, D.P. Dewitt, T.L. Bergman, A.S. Lavine, Fundamentals of Heat and Mass Transfer, 6th Edition, John Wiley & Sons, 2006.
[29] A. Bejan, Convection Heat Transfer, 3rd edition, John Wiley & Sons, Hoboken, 2004.